C. R. Physique 15 (2014) 898–906

Contents lists available at ScienceDirect

Comptes Rendus Physique

www.sciencedirect.com

The Sagnac effect: 100 years later / L'effet Sagnac : 100 ans après

Sagnac-based rotation sensing with superfluid helium quantum interference devices

Capteurs de rotation fondés sur l'effet Sagnac avec interférences quantiques dans l'hélium superfluide

Yuki Sato

Rowland Institute at Harvard, Harvard University, Cambridge, MA 02142, USA

ARTICLE INFO

Article history:
Available online 22 October 2014

Keywords:
Sagnac effect
Rotation sensing
Matter–wave interferometry
Superfluid helium
Josephson effects
Bose–Einstein condensate

Mots-clés :
Effet Sagnac
Capteurs de rotation
Interférométrie à onde de matière
Hélium superfluide
Effets Josephson
Condensat de Bose–Einstein

ABSTRACT

The Sagnac effect has played an instrumental role for the fundamental studies of relativity, and various devices that utilize this effect have been applied to many disciplines ranging from inertial navigation to geodesy and to seismology. In this context we present an overview of recent developments related to superfluid helium quantum interference devices. With the discovery of superfluid Josephson phenomena in ^{4}He, the device technology has been rapidly developing in the past 10 years. We discuss the underlying working principles of these interference devices and their applications. We focus on their use as sensitive rotation sensors based on the Sagnac effect coupled with the existence of a macroscopic quantum phase via particle–wave duality.

RÉSUMÉ

L'effet Sagnac a joué un rôle déterminant dans les études fondamentales en relativité, et les dispositifs utilisant cet effet ont trouvé des applications dans des disciplines variées allant, de la navigation inertielle à la géodésie et à la sismologie. Dans ce contexte, nous présentons un aperçu de l'évolution récente des dispositifs d'interférence quantique dans l'hélium superfluide. Avec la découverte de l'effet Josephson dans l'hélium 4 superfluide, cette technologie s'est rapidement développée au cours des dix dernières années. Nous discutons ici les principes sous-jacents à ces dispositifs d'interférences et leurs applications. Nous nous concentrons sur leur utilisation en tant que capteurs de rotation fondés sur l'effet Sagnac couplée avec l'existence d'une phase quantique macroscopique via la dualité particule–onde.

1. Sagnac effect

The Sagnac effect refers to a rotation-induced phase shift in interferometry [1,2]. The most well-known scenario appears in a laser interferometer where a beam of light is split in half and recombined again while enclosing a finite area A. When

E-mail address: sato@rowland.harvard.edu.

http://dx.doi.org/10.1016/j.crhy.2014.10.004
1631-0705/

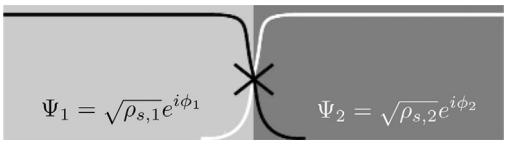

Fig. 1. A schematic depicting two superfluids joined at a junction (labeled X). Wavefunctions overlap and couple weakly across the junction. From Ref. [11].

the device is rotated at angular speed $\vec{\Omega}$ about an axis perpendicular to its plane $\hat{n}$, the path difference traveled by light in the general relativistic point of view leads to a phase shift

$$\Delta\phi_S = \frac{2\omega}{c^2}\vec{\Omega}\cdot\vec{A} \tag{1}$$

where $\vec{A}$ $(= A\hat{n})$ is the area vector of the device loop, c is the speed of light, and ω is the angular frequency. The equation above relates the rate of rotation applied to the apparatus to the experimental observable of the phase difference, effectively rendering the device a rotation sensor. The effect has been validated, and for optical interferometers it has seen applications in various forms including fiber optical and ring laser gyroscopes in fields ranging from inertial sensing to geodesy and to seismology [3–5].

In addition to the case of photons discussed above, as it became possible to split beams of particles and to have them recombine and interfere, the same general treatment has been applied to "massive" systems of neutrons, atoms, and superfluids [6–11]. Among these, all but the last category share the common operational characteristic that individual particles traverse the interferometer arms to recombine and interfere with themselves while the applied rotation affects the phase of traveling wavepackets. The superfluid device based on the exploitation of the Josephson phenomena is somewhat unique in that individual particles in the condensate essentially sit idle but they collectively interfere with themselves across the so-called Josephson junctions while the rotation acts on the macroscopic wavefunction phase to perturb this interference. Here we describe the physics of these superfluid helium quantum interference devices and their application and potential as Sagnac-based rotation sensors [11].

2. Superfluid helium and Josephson effects

Superfluid helium is an example of a macroscopic quantum system, a class that also includes superconductors and Bose–Einstein-condensed (BEC) gases. The overarching similarity in these systems is the existence of an "order parameter" with a well-defined overall phase. The existence of such a quantum state can be invoked using particle–wave duality of matter. All matter behaves as a wave with a characteristic wavelength that is inversely proportional to its momentum. Therefore as one cools a collection of atoms, their momentum decreases and the associated wavelength increases. At some point, the wavelength of each particle should become comparable to the interatomic distances, and the spatial extent of their presence starts to overlap with one another. The entire group of atoms then forms a single system that can only be thought of as one coherent probability cloud. The superfluid states of quantum liquids (^{3}He and ^{4}He) are described by a macroscopic wavefunction of the form $\Psi = \sqrt{\rho_s}e^{i\phi}$, where ρ_s is the superfluid density and ϕ is the quantum mechanical phase [12].

The interference device that is the topic of discussion here is based on a phenomenon that appears when two superfluids are weakly coupled together (see Fig. 1). Two superfluid reservoirs are joined at a junction labelled X. If the coupling between the two reservoirs is sufficiently weak, the two superfluids are described by two distinct wavefunctions $\Psi_R = \sqrt{\rho_{s,R}}e^{i\phi_R}$ and $\Psi_L = \sqrt{\rho_{s,L}}e^{i\phi_L}$. The time-dependent Schrodinger equation applied to this coupled system gives [13]:

$$i\hbar\frac{\partial\Psi_R}{\partial t} = \mu_R\Psi_R + \hbar\chi\Psi_L \tag{2}$$

and

$$i\hbar\frac{\partial\Psi_L}{\partial t} = \mu_L\Psi_L + \hbar\chi\Psi_R \tag{3}$$

where μ_R and μ_L denote the chemical potentials of the two reservoirs. The term $\hbar\chi$ represents the coupling across the junction, and it is defined such that χ has the dimension of frequency to give a measure of Ψ_R leaking into Ψ_L and vise versa. Inserting Ψ_R and Ψ_L into Eqs. (2) and (3) and defining the phase difference $\Delta\phi = \phi_R - \phi_L$ and the chemical potential difference $\Delta\mu = \mu_R - \mu_L$, one obtains two governing equations:

$$I = I_0\sin\Delta\phi \tag{4}$$

and

$$\frac{\partial\Delta\phi}{\partial t} = -\frac{\Delta\mu}{\hbar} \tag{5}$$

Eq. (4), often called the dc-Josephson equation [14], describes the nonlinear relation between the quantum phase difference across the junction and the superfluid mass current I that flows through it. This relation applies strictly to weakly coupled quantum systems. Eq. (5), often called the Josephson–Anderson phase evolution equation [15], states that the phase difference evolves in response to the chemical potential difference. Unlike Eq. (4), Eq. (5) is applicable to the time evolution of phase difference between any two locations in superfluids, whether weakly coupled or not.

If a fixed (i.e. constant) chemical potential difference is established between two weakly coupled superfluids, the phase difference increases linearly in time according to Eq. (5). Plugging this into Eq. (4) gives:

$$I = I_0 \sin \frac{\Delta\mu}{\hbar} t \tag{6}$$

Hence counterintuitively an oscillating mass current appears across the junction in response to a constant $\Delta\mu$, and its oscillation frequency is proportional to the applied $\Delta\mu$. We refer to this phenomenon as a Josephson oscillation and its frequency $f_J = \Delta\mu/h$ as the Josephson frequency. The junction in this context is often called a "weak link" to imply the nature of coupling although the term Josephson junction is also common. For superfluid helium, $\Delta\mu = m^*(\Delta P/\rho - s\Delta T)$ where ρ is the fluid density, s is the specific entropy, ΔP and ΔT are pressure and temperature differentials, and m^* is the effective mass of superfluid constituents, either the atomic mass of ^{4}He or twice the ^{3}He atomic mass [12].

3. Superfluid helium weak link

In superconducting systems a thin film of normal metal or insulator can be used as a weak link between two superconducting materials as electrons quantum-tunnel through such a barrier to establish the weak coupling required for the Josephson phenomena to emerge [14]. However the same approach cannot be employed for superfluid helium as helium atoms are too large to exhibit appreciable tunneling. To make a superfluid weak link, one needs to construct the equivalent of a Dayem Bridge [16], a constricted connection passage whose dimensions are on the order of the superfluid healing length ξ. This is the characteristic minimum length scale over which the wavefunction can change significantly, and superfluidity is effectively suppressed within this distance away from the wall. Two superfluid reservoirs joined through a passage of this length scale are therefore neither completely disconnected (and independent of each other) nor strongly connected (and virtually a single reservoir). Two reservoirs then form a weakly coupled quantum system. For ^{3}He, the healing length is given by [17]

$$\xi_3 = \frac{65\ \text{nm}}{(1 - T/T_c)^{1/2}} \tag{7}$$

where the superfluid transition temperature $T_c = 1$ mK. In contrast the healing length of ^{4}He is represented by [18]

$$\xi_4 = \frac{0.3\ \text{nm}}{(1 - T/T_\lambda)^{0.67}} \tag{8}$$

where the superfluid transition temperature $T_\lambda = 2.17$ K. While the temperature-dependent healing length for ^{3}He is typically on the order of tens of nanometers, it is typically two orders of magnitude smaller for ^{4}He. Naturally, when the field of micro/nano-fabrication advanced to feature sizes of tens of nanometers, the era of Josephson physics in superfluids began with ^{3}He. The first reports of a flow signature consistent with the Josephson current-phase relation came in 1988 from the team of Éric Varoquaux and Olivier Avenel in Saclay, France [19], followed by the direct observation of Josephson oscillations a decade later [20].

As for superfluid ^{4}He, early evidence of $\sin\phi$ current-phase behavior was finally reported in 2001 [21], followed by the direct observation of Josephson oscillations four years later [22]. Instead of attempting to fabricate sub-nanometer size apertures to match the zero-temperature healing length, these works took advantage of the diverging behavior of ξ_4 very close to T_λ as given in Eq. (8). This variation predicts $\xi_4 \sim 60$ nm when $T_\lambda - T \sim 1$ mK, which allowed the use of channels that could be fabricated with e-beam lithography. The ^{4}He Josephson work has progressed rapidly since then given the ease of cryogenics involved at 2 K compared to 1 mK required for superfluid ^{3}He.

4. Superfluid helium quantum interference device

A superfluid helium quantum interference device is a tool that exploits the Josephson oscillation phenomena discussed above (see Fig. 2 for a simplified device configuration). A torus filled with superfluid helium is interrupted by two weak links. Each weak link here is an array of apertures, and the array is used to amplify the overall oscillation signal to a detectable level. Here $\Delta\phi_1$ and $\Delta\phi_2$ denote the phase differences across the two weak links. For the wavefunction to be single-valued, the phase integral $\oint \nabla\phi \cdot d\vec{l}$ has to equal $2\pi n$ for the closed path taken along the torus. If a constant $\Delta\mu$ is applied across these weak links, mass currents $I_1 \sin\Delta\phi_1$ and $I_2 \sin\Delta\phi_2$ appear across the junctions according to Eq. (4),

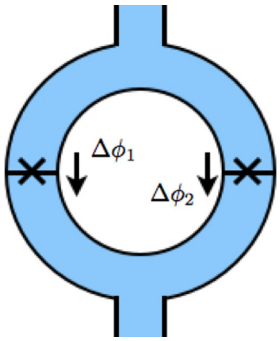

Fig. 2. (Color online.) A schematic view of the superfluid helium quantum interference device. A torus filled with superfluid helium is interrupted by two weak links. The phase differences between the two weak links are defined as $\Delta\phi_1$ and $\Delta\phi_2$ respectively. Each weak link is an array of nanoscale apertures.

while both $\Delta\phi_1$ and $\Delta\phi_2$ evolve in time according to Eq. (5). The total mass current $I = I_1 \sin\Delta\phi_1 + I_2 \sin\Delta\phi_2$ can be written as

$$I = I^* \sin\Delta\phi = I^* \sin\frac{\Delta\mu}{\hbar}t \tag{9}$$

where $\Delta\phi = (\Delta\phi_1 + \Delta\phi_2)/2$. If there exists some external phase shifting influence, the phase integral condition reads $\oint \vec{\nabla}\phi \cdot d\vec{l} = \Delta\phi_1 - \Delta\phi_2 + \Delta\phi_{\text{ext}} = 2\pi n$. Setting $n = 0$, one finds that the overall oscillation amplitude modulates according to

$$I_c^* = (I_1 + I_2)\sqrt{\cos^2\frac{\Delta\phi_{\text{ext}}}{2} + \gamma^2 \sin^2\frac{\Delta\phi_{\text{ext}}}{2}} \tag{10}$$

with $\gamma = (I_1 - I_2)/(I_1 + I_2)$. This is the operating principle of the superfluid helium quantum interference device. Quantum coherence within the superfluid leads to Josephson oscillations whose combined amplitude from two separated weak links provides a direct measure of the phase gradients present.

In the case of superconducting quantum interference devices [23], the phase shift $\Delta\phi_{\text{ext}}$ is induced by the change in the magnetic flux threading through the superconducting loop, making the device an extremely sensitive magnetometer. We show in the following section that, for the neutral superfluid counterpart, the role of magnetic flux can be played by the so-called rotation flux: $\vec{\Omega} \cdot \vec{A}$, rendering the device a sensitive rotation sensor.

5. Phase shift by rotation

Without much loss of generality, we first compute for massive particles a rotation-induced phase shift. Following Ref. [24], for a particle at location $\vec{r}$, the velocity in the inertial frame is related to that in the rotating frame via $\vec{v}' = \vec{v} + \vec{\Omega} \times \vec{r}$. Hence the Lagrangian can be written as

$$\begin{aligned} L(\vec{r}, \vec{v}) &= \frac{1}{2}m(\vec{v} + \vec{\Omega} \times \vec{r})^2 \\ &= \frac{1}{2}mv^2 + m\vec{\Omega} \cdot (\vec{r} \times \vec{v}) + \frac{1}{2}m(\vec{\Omega} \times \vec{r})^2 \end{aligned} \tag{11}$$

Neglecting the last higher-order term, the second term (Coriolis term) can be treated as the sole perturbation to the Lagrangian compared to the free-particle scenario. The extra phase accumulated can then be computed by the action integral:

$$\Delta\phi = \frac{1}{\hbar}\oint \Delta L dt = \frac{m}{\hbar}\vec{\Omega} \cdot \oint (\vec{r} \times \vec{v}) dt = \frac{m}{\hbar}\vec{\Omega} \cdot \oint \vec{r} \times d\vec{r} = \frac{2m}{\hbar}\vec{\Omega} \cdot \vec{A} \tag{12}$$

where A represents the area swept by the particle trajectory $\vec{r}$. This phase shift, obtained pseudo-classically above, corresponds to the Sagnac phase shift for massive particles. See Refs. [25,26] for a more relativistic motivation for the effect and the derivation of the rotation-induced Lagrangian terms for matter waves via fully general-relativistic equations.

With a general solution in hand, we now turn to the case specific to a superfluid helium quantum interference device. Let's first consider the simplest scenario of rotating the device about the area vector of the torus so that $\vec{\Omega} \parallel \vec{A}$ as depicted in Fig. 3. Due to the existence of partitions containing weak links, fluid flow similar to solid-body motion $|v_s| \approx \Omega R$ (where R is the major radius of the torus) will be induced in the region away from the weak link junctions. Applying the current operator $J = -(i\hbar/2m)(\Psi^*\vec{\nabla}\Psi - \Psi\vec{\nabla}\Psi^*)$ to a wavefunction of the form $\Psi = \sqrt{\rho_s}e^{i\phi}$, the phase gradient in these regions is related to superfluid velocity via $\vec{\nabla}\phi = (m/\hbar)\vec{v}_s$ [12]. Using these relations, a closed path integral of the phase gradient along the torus can be divided into four parts and computed as

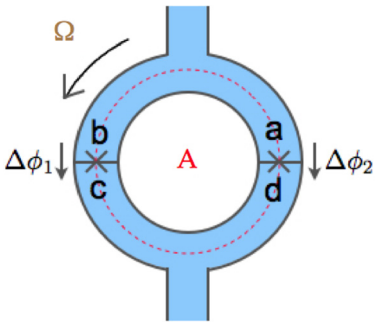

Fig. 3. (Color online.) A schematic view of the superfluid helium quantum interference device with a sensing area A. The device is rotated about the area vector of the torus with angular speed Ω. In this example, $\vec{\Omega} \parallel \vec{A}$, and both vectors point out of the page. Symbols a, b, c, and d denote the starting and ending locations for sectional path integrals defined in the text. The dotted line depicts the integral path.

$$\begin{aligned}\oint \vec{\nabla}\phi \cdot \mathrm{d}\vec{l} &= \int_a^b \vec{\nabla}\phi \cdot \mathrm{d}\vec{l} + \int_b^c \vec{\nabla}\phi \cdot \mathrm{d}\vec{l} + \int_c^d \vec{\nabla}\phi \cdot \mathrm{d}\vec{l} + \int_d^a \vec{\nabla}\phi \cdot \mathrm{d}\vec{l} \\ &= \frac{m}{\hbar}\int_a^b \vec{v}_s \cdot \mathrm{d}\vec{l} + \Delta\phi_1 + \frac{m}{\hbar}\int_c^d \vec{v}_s \cdot \mathrm{d}\vec{l} - \Delta\phi_2 \\ &= \frac{2m}{\hbar}\Omega A + \Delta\phi_1 - \Delta\phi_2 \end{aligned} \tag{13}$$

where A is the area enclosed by the integrals over $\vec{v}_s$ along the two main arms of the interferometer, which equals the device area. In a more general scenario where $\vec{\Omega} \nparallel \vec{A}$, the product of the angular speed and the sensing area needs to be generalized by the vector dot product such that

$$\oint \vec{\nabla}\phi \cdot \mathrm{d}\vec{l} = \frac{2m}{\hbar}\vec{\Omega} \cdot \vec{A} + \Delta\phi_1 - \Delta\phi_2 \tag{14}$$

Comparing the above result with the phase integral contributions for the non-rotating case: $\oint \vec{\nabla}\phi \cdot \mathrm{d}\vec{l} = \Delta\phi_1 - \Delta\phi_2$, it can be seen that the Sagnac phase shift introduced by the application of finite rotation to the superfluid interferometer is given by

$$\Delta\phi_S = \frac{2m}{\hbar}\vec{\Omega} \cdot \vec{A} \tag{15}$$

which agrees with Eq. (12).

It is instructive to compare this result with the optical Sagnac phase shift given by Eq. (1). One sees that the two are identical except that the effective photon mass $\hbar\omega/c^2$ is replaced by the helium atomic mass, which is 10^{10} times heavier. Thus for the same change in the rotation rate, the signal from the helium device would be 10 orders of magnitude larger compared to optical devices with the same sensing area. Although it is nontrivial to imagine constructing a superfluid device that spans hundreds of meters across in footprint as have been done with ring laser and fiber optical gyros, the signal size ratio of ten billion for the same device dimensions suggests immense potential for compact and yet ultrasensitive rotation sensors.

Setting $\oint \vec{\nabla}\phi \cdot \mathrm{d}\vec{l} = 2\pi n$ with $n = 0$ in Eq. (14), the total mass current can be written as in Eqs. (9) and (10) where $\Delta\phi_{\mathrm{ext}}$ is now given by the Sagnac phase shift $\Delta\phi_S$. Quantum interference has been observed in both ^{3}He and ^{4}He, and the underlying principle has been tested by inducing and detecting the Sagnac phase shift arising from the spinning Earth. Fig. 4 shows such interference pattern obtained with a ^{4}He quantum interference device [10]. Through the Sagnac effect acting on the macroscopic wavefunction phase with the phase integral requirement, a superfluid interferometer becomes a rotation sensor.

We note that the discussion on the novel oscillation phenomenon and its utilization for interferometry has thus far focused on the regime where two superfluid reservoirs are weakly coupled. For superfluid ^{4}He, as the temperature is lowered and the healing length becomes much smaller than the aperture dimensions, Josephson oscillations cease to exist. However it turns out that a different type of oscillation (based on the physics of "phase slippage") emerges at the Josephson frequency, enabling the operation of superfluid interferometry even in the regime where two superfluid reservoirs are strongly connected. For details on the nature of fluid oscillations in these two distinct regimes as well as the intermediate cross-over regime, we refer readers to Ref. [27].

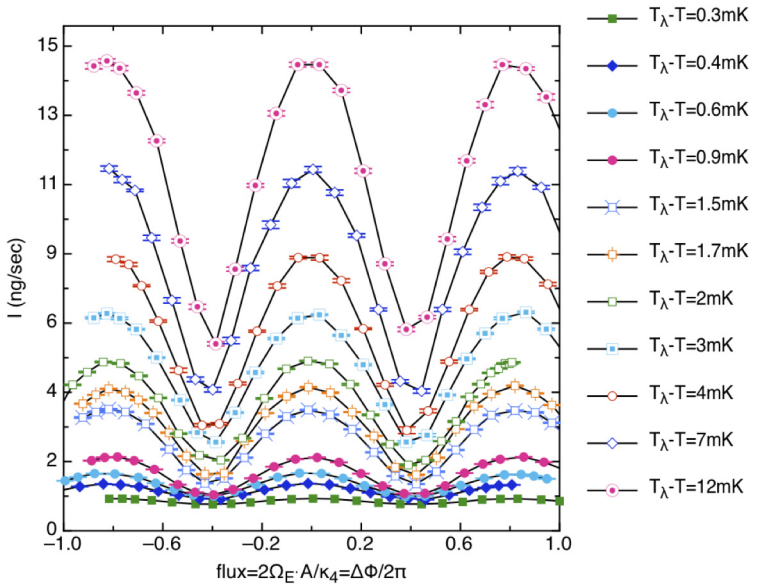

Fig. 4. (Color online.) Modulation of the Josephson oscillation amplitude as a function of rotation flux $\vec{\Omega} \cdot \vec{A}$ in a superfluid ^{4}He matter-wave interferometer. The Earth is the source of rotation flux, and its magnitude is varied by reorienting the interferometer with respect to the north–south axis of the Earth. From Ref. [10].

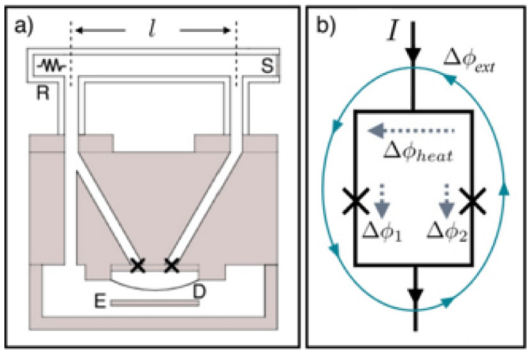

Fig. 5. (Color online.) a) Experimental apparatus depicting a flux-locked rotation sensor. The inside is filled with superfluid ^{4}He and the entire apparatus is immersed in a bath of liquid helium. The heat injected at R induces a phase shift $\Delta\phi_{\text{heat}}$ across the top arm of interferometer loop. S represents a heat sink. Diaphragm (D) and electrode (E) form a sensitive sensor for fluid motion in the weak links. b) Equivalent SQUID circuit. $\Delta\phi_{\text{ext}}$ is the overall phase shift that the interferometer is being used to measure. $\Delta\phi_1$ and $\Delta\phi_2$ are the phase differences across the two weak links and $\Delta\phi_{\text{heat}}$ is the phase shift due to injected heater power. When the device is rotated, the Sagnac phase shift appears in addition to the above phase shifts. From Ref. [28].

6. Flux modulation and feedback circuit for rotation sensing

Interferometers almost invariably have a transfer function wherein the device output is a nonlinear function of some variable of interest. A cosinusoidal transfer function such as Eq. (10) is one of the most typical cases encountered. The device sensitivity then varies depending on the size of the signal that it detects, which significantly hinders the utility of the device. Moreover due to the periodicity of the device output exemplified by the data shown in Fig. 4, large changes in signal can be determined only by tracing the whole interference pattern in real time, which is temporally impractical. For these reasons, it is critical to be able to linearize the device to have an output that is directly proportional to the variable of interest. Although such linearization of the instrument response remains nontrivial for most interferometric devices, a novel scheme has been developed for a superfluid helium quantum interference device [28].

Fig. 5a displays an interferometer loop in which one arm is a straight tube of length l and cross-sectional area σ containing a heater (R) at one end and a heat sink (S) at the other. According to the two-fluid model [12], when power $\dot{Q}$ is applied to the heater, the normal component flows away from the heat source with velocity v_{n} while the superfluid counterflow is established with velocity:

$$|v_{\text{s}}| = \frac{\rho_{\text{n}}}{\rho\rho_{\text{s}} T s \sigma} \dot{Q} \tag{16}$$

where ρ, ρ_s, and ρ_n are the total, super, and normal fluid densities respectively. Through the relation $\vec{\nabla}\phi = (m/\hbar)\vec{v}_s$, the application of heat corresponds to an injection of phase shift into the interferometer arm [29]:

$$\Delta\phi_{\text{heat}} = \frac{l}{\sigma}\frac{m}{\hbar}\frac{\rho_n}{\rho\rho_s Ts}\dot{Q} \tag{17}$$

Various phase contributions in the absence of rotation are depicted schematically in Fig. 5b. When there exists external rotation, both the Sagnac phase shift and the heat current phase shift are picked up by the device. In that scenario, any change in rotation flux can be canceled by injecting heater power so that the overall phase shift $\Delta\phi_{\text{ext}} = \Delta\phi_S + \Delta\phi_{\text{heat}}$ remains constant. A heat-induced phase shift works as a flux modulator, and the interferometer output can be maintained at a fixed amplitude and the flux is locked. This allows one to bias the device at the point of the greatest slope and operate there without having to trace many interference cycles arising from large changes in rotation flux. Furthermore, the amount of power needed for this feedback provides a linear measure of the change in rotation flux: $|\vec{\Omega}\cdot\vec{A}| = a\dot{Q} + \text{const.}$ where $a \equiv l\rho_n/(2\sigma\rho\rho_s Ts)$.

Fig. 6 demonstrates this flux-locked rotation sensing. When the interferometer is reoriented about the vertical, changing the angle between the device's area vector and the Earth's spin axis, the instrument's output exhibits a signature Sagnac interference shown in Fig. 6a. In panel b, the feedback is turned on to nullify the Sagnac phase shift with the injected heat current. The device shows a constant mass current amplitude even when it is reorientated with respect to the Earth's rotation vector. When the heater power required for this feedback is plotted against the rotation flux (Fig. 6c), it can be clearly seen that the technique provides a linear measure of the variable of interest while the sensitivity is now constant and independent of the rotation flux.

7. Rotational sensitivity

With several proof-of-concept devices already implemented, it is natural to ask how sensitive these rotation sensors can be. In 2011, a large-area multi-turn superfluid ^{4}He interferometer was reported [30]. The device's arm consisted of four turns in astatic configuration to make gradiometric phase shift measurements, and the interfering path length was 0.5 m, enclosing the total area of 200 cm^2. The intrinsic rotational sensitivity of this particular device (if the path of the same length was wound in one direction) is reported to be $\sim 10^{-8}$ rad/s in 1 second measurement time. Although this sensitivity is already quite high, there is much room for significant improvement as the rotational sensitivity of a superfluid helium quantum interference device depends on several parameters including the number of apertures in a junction, sensing area per turn of the interferometer arm, and the number of the overall turns. For example a single superfluid weak link typically contains roughly 5000 nanoscale apertures in a 200 μm by 200 μm SiN membrane. An increase in the number of apertures by an order of magnitude is easily feasible with the current *e*-beam technology, and it is projected that the signal increase just from that alone could make this device one of the most sensitive matterwave-based rotation sensors reported.

The parameters mentioned above in relevance to the device sensitivity are those that have to do with the instrument configuration and geometry. Much sensitivity improvement is also expected from exploiting nonlinear Josephson dynamics. Flux-locking discussed in the previous section is an example of making an effective use of a novel physical phenomenon to enhance the utility of the instrument. Similarly many nonlinear phenomena have been reported that could be used to enhance the sensitivity significantly [31,32]. The so-called Fiske effect which occurs in the mixing of Josephson oscillations with the local acoustic resonances of the apparatus has been demonstrated to increase the signal to noise ratio by a factor as much as 30 [33]. With further work it may be possible to even engineer sharp acoustic resonances to further take advantage of this robust amplification mechanism. A phenomenon called bifurcation has also been reported in the resonance of superfluid Josephson systems with a potential to create a novel amplifier based on hysteretic switching of signal amplitudes [34].

Configured as a phase meter, the ultimate phase resolution limit of superfluid-based interferometers may be quantum fluctuations embodied in the uncertainty principle. With $\sim 10^{23}$ atoms involved in the device and a large area made possible by the macroscopic nature of the quantum liquid, superfluid devices may be advantageous in comparison to those based on BEC gases [35,36]. However, that ultimate resolution will always be masked by the vibrational noise from the environment. Although a simple translation will not correspond to signal changes, any small tilting of the instrument can lead to rotational noises. In applications such as geodetic gyroscopy, placing the devices in an underground low vibration laboratory may be a necessity to mitigate any background signals as the ultimate sensitivity is explored. On the other hand in scenarios such as inertial navigation where the noisy environment is expected, the flux-locking technique would have to be developed further with a slew rate high enough to track nuisance signals.

As mentioned previously the exquisite sensitivity per device size raises an interesting potential as a compact rotation sensor that can be moved from one location to another. As a fixed instrument, it will be fascinating to see whether or not the sensitivity can be raised further to complement the world's most sensitive ring laser gyroscopes in their study of minute variations in the Earth's rotation as well as their quest for terrestrial tests of frame dragging from the spinning Earth [5]. Besides simple bench-marking between different platforms, it will be fascinating to tackle an experiment where beams of light and matter respond quite differently to not only learn about a particular phenomenon of interest but also to gain insights into various similarities and dissimilarities that exist among these instruments.

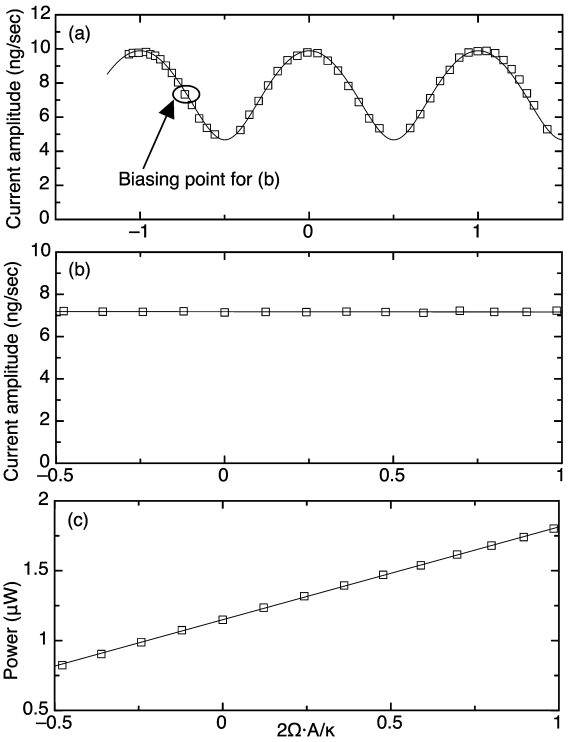

Fig. 6. a) Interferometer output as a function of the Earth's rotation flux in the absence of heater-induced phase biasing. b) The modulation in the interferometer signal is compensated by injected heater current, making the amplitude independent of the rotation flux. The amplitude is maintained constant at the bias point circled in panel a. c) Feedback heater power used for a given value of the rotation flux to flux-lock the interferometer. From Ref. [28].

8. Conclusion

In 1913 George Sagnac split a beam of light, counter-propagated the beams along the same optical path, and demonstrated that the shift in the interferometry pattern was directly proportional to the rate of rotation applied to the apparatus. This observation is now known as the Sagnac effect, and over the past hundred years it has seen applications in many disciplines ranging from inertial navigation to seismology. In this context we have presented an overview of recent developments related to superfluid helium quantum interference devices. In these novel devices, atoms in the condensate sit idle but collectively interfere with themselves across two weak links to produce Josephson oscillations. Through the Sagnac effect the externally applied rotation shifts the macroscopic wavefunction phase to affect this interference, altering the amplitude of the mass current oscillations and rendering the device a sensitive matter-wave rotation sensor. With quantum phase fluctuations being the ultimate limiting factor in the gyroscope's performance, these superfluid devices form viable candidates for high precision rotation sensing along with state-of-the-art laser and atom interferometers. See Ref. [11] for more details related to the physics and applications of superfluid helium quantum interference devices. For discussion on related superfluid gyrometers based on a single junction and a large parallel path, see Ref. [8].

References

[1] G. Sagnac, C. R. Acad. Sci. Paris 157 (1913) 708.
[2] E.J. Post, Rev. Mod. Phys. 39 (1967) 475.
[3] H. Lefevre, The Fiber-Optic Gyroscope, Artech House, Boston, 1993.
[4] K.U. Schreiber, et al., Pure Appl. Geophys. 166 (2007) 1485.
[5] K.U. Schreiber, J.P.R. Wells, Rev. Sci. Instrum. 84 (2013) 041101.
[6] S.A. Werner, et al., Phys. Rev. Lett. 42 (1979) 1103.
[7] T.L. Gustavson, et al., Class. Quantum Gravity 17 (2000) 2385.
[8] O. Avenel, et al., J. Low Temp. Phys. 135 (2004) 745.
[9] R. Simmonds, et al., Nature 412 (2001) 55.
[10] E. Hoskinson, et al., Phys. Rev. B 74 (2006) 100509(R).
[11] Y. Sato, R.E. Packard, Rep. Prog. Phys. 75 (2012) 016401.
[12] D.R. Tilley, J. Tilley, Superfluidity and Superconductivity, Institute of Physics, Bristol, UK, 1990.
[13] R.P. Feynman, et al., The Feynman Lectures in Physics, vol. 3, Addison-Wesley, Reading, UK, 1963.
[14] K.K. Likharev, Dynamics of Josephson Junctions and Circuits, Academic Press, New York, 1986.
[15] P.W. Anderson, Rev. Mod. Phys. 38 (1966) 298.
[16] P.W. Anderson, A.H. Dayem, Phys. Rev. Lett. 13 (1988) 195.

[17] D. Vollhardt, P. Wolfle, The Superfluid Phases of Helium-3, Taylor and Francis, New York, 1990.
[18] R.P. Henkel, et al., Phys. Rev. Lett. 23 (1969) 1276.
[19] O. Avenel, E. Varoquaux, Phys. Rev. Lett. 60 (1988) 416.
[20] S.V. Pereverzev, et al., Nature 388 (1997) 449.
[21] K. Sukhatme, et al., Nature 411 (2001) 280.
[22] E. Hoskinson, et al., Nature 433 (2005) 376.
[23] J. Clarke, A.I. Braginski, The SQUID Handbook: Fundamentals and Technology of SQUIDs and SQUID Systems, Wiley-VCH, Weinheim, Germany, 2004.
[24] P. Storey, C.C. Tannoudji, J. Phys. II 4 (1994) 1999.
[25] B.H.W. Hendriks, G. Nienhuis, Quantum Opt. 2 (1990) 13.
[26] E. Varoquaux, G. Varoquaux, Phys. Usp. 51 (2008) 205.
[27] E. Hoskinson, et al., Nat. Phys. 2 (2005) 23.
[28] Y. Sato, et al., Appl. Phys. Lett. 91 (2007) 074107.
[29] Y. Sato, et al., Phys. Rev. Lett. 98 (2007) 195302.
[30] S. Narayana, Y. Sato, Phys. Rev. Lett. 106 (2001) 255301.
[31] E. Hoskinson, et al., AIP Conf. Proc. 850 (2006) 117.
[32] A. Joshi, R.E. Packard, J. Low Temp. Phys. 172 (2013) 162.
[33] Y. Sato, Phys. Rev. B 81 (2010) 172502.
[34] S. Narayana, Y. Sato, Phys. Rev. Lett. 105 (2010) 205302.
[35] K.C. Wright, et al., Phys. Rev. Lett. 110 (2013) 025302.
[36] C. Ryu, et al., Phys. Rev. Lett. 111 (2013) 205301.